Roles of Cholesterol in Early and Late Steps of the Nipah Virus Membrane Fusion Cascade

Erik M. Contreras,[a] Gunner P. Johnston,[a] David W. Buchholz,[a] Victoria Ortega,[a] I. Abrrey Monreal,[a] J. Lizbeth R. Zamora,[a] Tracy Cheung,[a] Hector C. Aguilar[a]

[a]Department of Microbiology and Immunology, College of Veterinary Medicine, Cornell University, Ithaca, New York, USA

Gunner P. Johnston and David W. Buchholz contributed equally to the manuscript.

ABSTRACT Cholesterol has been implicated in various viral life cycle steps for different enveloped viruses, including viral entry into host cells, cell-cell fusion, and viral budding from infected cells. Enveloped viruses acquire their membranes from their host cells. Although cholesterol has been associated with the binding and entry of various enveloped viruses into cells, cholesterol's exact function in the viral-cell membrane fusion process remains largely elusive, particularly for the paramyxoviruses. Furthermore, paramyxoviral fusion occurs at the host cell membrane and is essential for both virus entry (virus-cell fusion) and syncytium formation (cell-cell fusion), central to viral pathogenicity. Nipah virus (NiV) is a deadly member of the *Paramyxoviridae* family, which also includes Hendra, measles, mumps, human parainfluenza, and various veterinary viruses. The zoonotic NiV causes severe encephalitis, vasculopathy, and respiratory symptoms, leading to a high mortality rate in humans. We used NiV as a model to study the role of membrane cholesterol in paramyxoviral membrane fusion. We used a combination of methyl-beta cyclodextrin (MβCD), lovastatin, and cholesterol to deplete or enrich cell membrane cholesterol outside cytotoxic concentrations. We found that the levels of cellular membrane cholesterol directly correlated with the levels of cell-cell fusion induced. These phenotypes were paralleled using NiV/vesicular stomatitis virus (VSV)-pseudotyped viral infection assays. Remarkably, our mechanistic studies revealed that cholesterol reduces an early F-triggering step but enhances a late fusion pore formation step in the NiV membrane fusion cascade. Thus, our results expand our mechanistic understanding of the paramyxoviral/henipaviral entry and cell-cell fusion processes.

IMPORTANCE Cholesterol has been implicated in various steps of the viral life cycle for different enveloped viruses. Nipah virus (NiV) is a highly pathogenic enveloped virus in the *Henipavirus* genus within the *Paramyxoviridae* family, capable of causing a high mortality rate in humans and high morbidity in domestic and agriculturally important animals. The role of cholesterol for NiV or the henipaviruses is unknown. Here, we show that the levels of cholesterol influence the levels of NiV-induced cell-cell membrane fusion during syncytium formation and virus-cell membrane fusion during viral entry. Furthermore, the specific role of cholesterol in membrane fusion is not well defined for the paramyxoviruses. We show that the levels of cholesterol affect an early F-triggering step and a late fusion pore formation step during the membrane fusion cascade. Thus, our results expand our mechanistic understanding of the viral entry and cell-cell fusion processes, which may aid the development of antivirals.

KEYWORDS Nipah virus, membrane, entry, fusion, paramyxovirus, henipavirus, cholesterol

Many enveloped viruses require membrane cholesterol for viral binding and entry into host cells (1, 2). Thus, the role(s) of cholesterol in virus entry has been investigated for several families of enveloped viruses, including DNA and positive RNA viruses. Similarly, the role of membrane cholesterol in the localization of viral proteins to liquid-ordered domains for assembly and viral particle release has also been well studied (3). For example, membrane cholesterol has been reported to have an essential role in human immunodeficiency virus (HIV) pathogenesis (4, 5). The retrovirus HIV-1 requires cellular cholesterol for viral particles to bind cells and for proper assembly, budding, and viral internalization (5–8). Herpesvirus requires membrane cholesterol for particle stability, infectivity, and cell-to-cell transmission of infection (9, 10). The infectivity of the orthomyxovirus influenza A/WSN/33 (H1N1) was reduced by methyl-beta cyclodextrin (MβCD) in a dose-dependent manner (11). In the *Pneumoviridae* family, respiratory syncytial virus (RSV) uses cholesterol-rich domains for virus-cell fusion, in addition to viral particle release (12, 13). The paramyxovirus avian paramyxovirus 1, also known as Newcastle disease virus (NDV), requires cholesterol in the target cell membrane for optimal virus entry. However, when cholesterol was directly depleted from the NDV membrane, entry was not affected. Conversely, NDV particles from cholesterol-depleted cells displayed a reduction in infectivity. Furthermore, cell-cell fusion in cholesterol-depleted cells was not inhibited (14–16). Cholesterol depletion of canine distemper virus (CDV) membranes reduced infectivity, while depletion of cellular cholesterol in infected cells reduced syncytium formation. However, cholesterol depletion in the target membrane did not reduce CDV entry (17). Finally, the infectivity of bovine parainfluenza virus type 3, human parainfluenza virus type 3, and Sendai virus was negatively affected by viral membrane cholesterol depletion with MβCD (18–20).

The role(s) of membrane cholesterol in Nipah virus (NiV) membrane fusion has not been previously explored. Most notably, although significant functions of membrane cholesterol during viral entry of enveloped viruses have been reported, the precise mechanistic step(s) by which cholesterol affects cell entry of the enveloped negative-sense single-stranded RNA viruses, including the paramyxoviruses, remains largely unexplored. We used NiV as an important model to determine how cholesterol affects paramyxoviral infections. We explored the role(s) of cholesterol in NiV entry and cell-cell fusion induced by NiV glycoproteins by performing a series of assays to dissect the steps of the membrane fusion cascade affected by NiV. Within the *Paramyxoviridae* family, NiV is in the *Henipavirus* genus, which includes 20 newly discovered viruses, primarily in bats (21). NiV causes encephalitis and respiratory disease and has a mortality rate of 40 to 100% in humans (22, 23). NiV is carried by members of the *Pteropus* genus of bats and can infect many mammals, including pigs, horses, dogs, and humans. Based on its broad mammalian tropism, the lack of an approved vaccine or effective antiviral therapeutic agent, and its high mortality rate in humans, NiV is classified as a biosafety level 4 agent (24).

NiV primarily enters cells via virus-cell membrane fusion at the plasma membrane. Cellular expression of the NiV glycoproteins can induce cell-cell membrane fusion (syncytium formation) by the cooperation of the attachment (G) and fusion (F) glycoproteins. The fusion of virus and host cell membranes is pH independent and begins with the binding of G to its host receptor ephrinB2 or ephrinB3 (25). Binding of G to ephrinB2/B3 initiates receptor-induced conformational changes within G, in turn inducing a conformational cascade in F (26–29). F transitions from its prefusion (PF) to its prehairpin intermediate (PHI) conformations, causing the fusion peptide to be inserted into the host cell membrane (30). Next, F progresses to the thermodynamically stable six-helix bundle (6HB) conformation, a transition that drives membrane fusion. For membrane fusion to go to completion, several intermediate steps must occur, including outer leaflet fusion (hemifusion), fusion pore formation, and fusion pore expansion (31). These critical steps in the membrane fusion cascade are necessary to initiate the infection of naive cells by either virus entry or cell-cell fusion.

Here, we reveal the role of membrane cholesterol in NiV cell-cell and virus-cell

membrane fusion. Notably, we also identify the importance of membrane cholesterol in early and late steps during the membrane fusion cascade. Using a variety of biochemical assays, we determine that not only cell-cell fusion and viral entry but also, more specifically, the levels of NiV F triggering and the extent of fusion pore formation are affected when membrane cholesterol levels are altered.

RESULTS

Depleting cellular cholesterol in NiV F/G-transfected cells reduces syncytium formation. To determine the role of cholesterol in NiV membrane fusion, we first assessed how lowering cholesterol levels would alter syncytium formation (cell-cell fusion), an important pathognomonic marker of paramyxoviral and NiV infections (32). Importantly, we decreased membrane cholesterol levels as biochemically gently as possible compared to studies performed with other viruses (2, 33, 34). Treatment was performed at 4 to 6 h posttransfection before syncytia could be visualized. Briefly, we transfected HEK293T cells with NiV F and G expression plasmids and then treated the cells with increasing concentrations of MβCD for 1 h at room temperature to remove cholesterol from the cell membranes. MβCD sequesters cholesterol solely from the plasma membrane, where the majority of cholesterol is found in the cell (35). The cells were then washed with phosphate-buffered saline (PBS) and allowed to recover from the relatively harsh MβCD treatment while being incubated with 10 μM lovastatin in serum-free medium during the remaining hours posttransfection, before cell collection. Lovastatin treatment was used to inhibit *de novo* synthesis of cholesterol, and equivalent dimethyl sulfoxide (DMSO) concentrations were used as mock treatments, as in previous studies (15, 36–38). The levels of cholesterol decreased with increasing concentrations of MβCD used such that treatment with 10 mM MβCD and 10 μM lovastatin resulted in a reduction in membrane cholesterol by 40% ($P = 0.0002$) (Fig. 1A). Notably, these treatments did not alter the cells' viability, as determined by a cell-counting kit 8 (CCK8) cell viability assay at such drug concentrations (Fig. 1B).

Importantly, a reduction in cholesterol levels resulted in a reduction in syncytium formation, in a dose-dependent fashion, whereby 60% cholesterol correlated with ~30% cell-cell fusion ($P < 0.0001$) (10 mM MβCD), compared to mock-treated cells (Fig. 1C). Cell-cell fusion was counted as the number of nuclei inside syncytia per random field at a ×200 magnification and normalized to the levels in mock-treated cells. Examples of syncytium fields are shown, with examples of syncytium nuclei counted circled in red (Fig. 1D). After observing that decreasing the concentration of membrane cholesterol affected the levels of syncytium formation, we then assessed whether decreased expression of F and G upon cholesterol reduction may be the cause of this effect. We thus transfected and treated HEK293T cells to express F and G, varied the cells' levels of cholesterol as described above, and then measured the levels of cell surface expression (CSE) of F and G and the ability of G to bind ephrinB2 under altered cholesterol conditions. We used rabbit polyclonal antibody 835 against NiV F and an antihemagglutinin (anti-HA) monoclonal antibody to detect HA-tagged NiV G, as we previously performed (39–41). We observed that cholesterol depletion did not significantly alter CSE levels of F or G when cotransfected. Furthermore, using purified soluble ephrinB2 fused to human Fc, we measured the ability of G to bind ephrinB2, as we previously performed (28, 41, 42). When cotransfected with F, the ability of G to bind ephrinB2 was unaltered when membrane cholesterol was reduced (Fig. 1E). We also tested if the levels of F cleavage were altered by cholesterol depletion. We observed that cleavage of NiV F in cholesterol-depleted cells was not altered compared to mock-treated cells (Fig. 1F). Altogether, these results suggest that reducing cellular membrane cholesterol decreased the levels of NiV-induced cell-cell fusion and that such a decrease was not due to altered cell viability, decreased CSE levels of NiV F or G, decreased levels of F cleavage, or decreased levels of ephrinB2 receptor binding to NiV G.
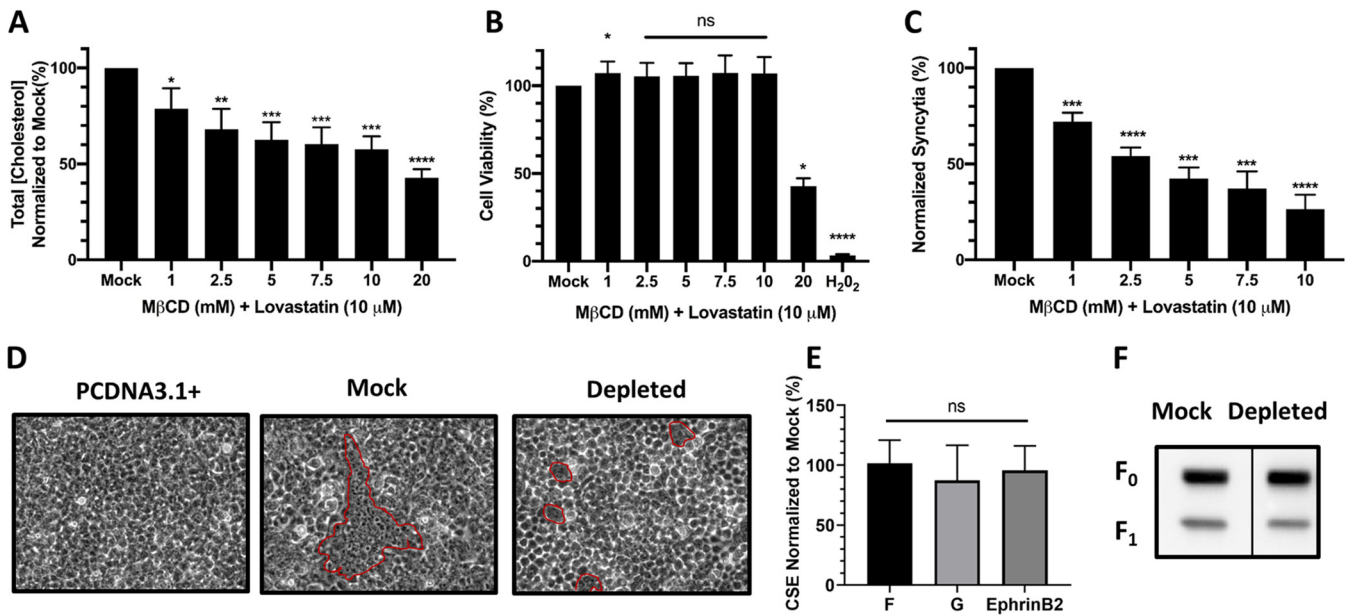
FIG 1 Depleting cellular cholesterol reduces cell-cell fusion. (A) The total cellular cholesterol concentration was measured with an Amplex red cholesterol kit after treatment with MβCD and 10 μM lovastatin. Cholesterol concentrations were normalized to those in mock-treated cells. (B) NiV F/G-transfected HEK293T cells were treated with increasing concentrations of MβCD and 10 μM lovastatin. Cytotoxic positive-control cells were treated with H_2O_2 at 0.3%. Viability was quantified with CCK8 that measures dehydrogenase activity in live cells. Cholesterol levels and cell viability were measured 9 to 12 h after treatment. (C) The levels of cell-cell fusion were quantified by counting the syncytia formed. The minimum numbers of nuclei inside syncytia were counted, considering a syncytium as having 4 or more nuclei within a common cell membrane. Nuclei in syncytia per random $\times$200 field were normalized to the no-treatment mock control, set at 100%. (D) Representative fields of syncytia, after treatment with 10 mM MβCD and 10 μM lovastatin, circled in red. (E) The levels of CSE of NiV F after cholesterol depletion were measured using polyclonal rabbit antibody 835 against NiV F (39, 40). G was detected using a monoclonal anti-HA phycoerythrin (PE) antibody. After the removal of membrane cholesterol, the levels of ephrinB2 binding to NiV G were measured using soluble ephrinB2 fused to human Fc. (F) Representative Western blot analysis of NiV F expression and cleavage of mock-treated and cholesterol-depleted cells. Data shown are averages from three independent experiments $\pm$ standard deviations (SD). Statistical significance was determined with a one-sample t test. *, $P < 0.05$; **, $P < 0.01$; ***, $P < 0.001$; ****, $P < 0.0001$; ns, not significant.

Increasing cellular cholesterol in NiV F/G-transfected cells increases syncytium formation. Since we observed a substantial decrease in syncytium formation in cholesterol-depleted cells expressing NiV F and G, we then tested if cholesterol enrichment would have the opposite effect on NiV-induced cell-cell fusion. Thus, we used a combination of cholesterol/MβCD (at a 1:20 ratio) to increase the concentration of membrane cholesterol (35, 43, 44). With increasing concentrations of cholesterol/MβCD, we observed a dose-dependent increase in cellular cholesterol of up to ~160% with 5 mM cholesterol/MβCD treatment compared to the mock treatment ($P = 0.0006$). All the following experiments utilizing cholesterol enrichment were thus performed at this concentration (Fig. 2A). Notably, this treatment did not negatively affect cell viability, as determined by CCK8 (Fig. 2B).

Importantly, treatment with 5 mM cholesterol/MβCD also increased the levels of syncytium formation to ~160% compared to the mock control cells ($P = 0.0034$) (Fig. 2C). Examples of syncytium formation are shown, with examples of nuclei counted circled in red (Fig. 2D). We then sought to determine if this increase in syncytium formation was caused by increased expression of F or G upon cholesterol enrichment. We observed that increased levels of syncytium formation were not caused by enhanced levels of F or G CSE. Furthermore, with the use of purified soluble ephrinB2 fused to human Fc, we observed that cholesterol enrichment did not alter the ability of G to bind ephrinB2 (Fig. 2E). We also tested if the levels of F cleavage were altered by cholesterol enrichment. We observed that cleavage of NiV F in cholesterol-enriched cells was not altered compared to the mock-treated cells (Fig. 2F). Altogether, our data indicated that increasing the concentration of cell membrane cholesterol increased the levels of NiV-induced syncytium formation but not as a result of altered cell viability, increased CSE levels of F or G, increased levels of F cleavage, or increased levels of receptor binding to NiV G.
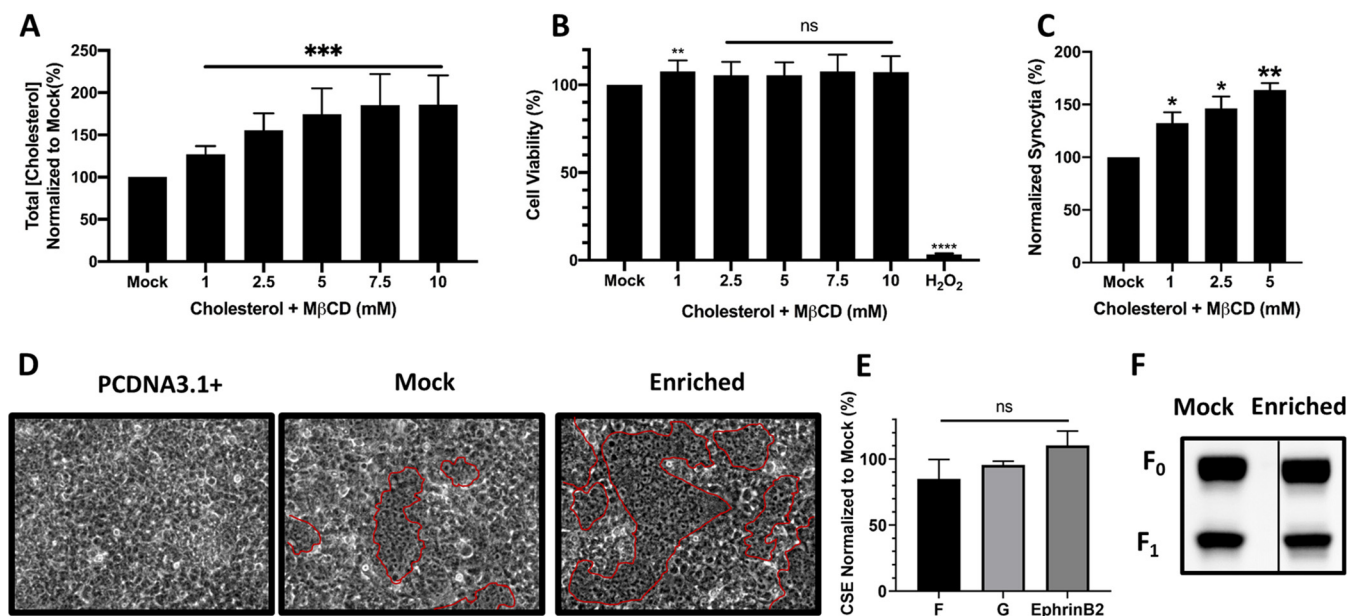
FIG 2 Enriching cellular cholesterol increases cell-cell fusion. (A) The total cellular cholesterol concentration was measured with an Amplex red cholesterol kit after treatment with increasing concentrations of a cholesterol/MβCD (1:20) solution. Cholesterol concentrations were normalized to those in mock-treated cells. (B) NiV F/G-transfected HEK293T cells were treated with increasing concentrations of cholesterol/MβCD. Cytotoxic positive-control cells were treated with H₂O₂ at 0.3%. Viability was quantified with CCK8 that measures dehydrogenase activity in live cells. Cholesterol levels and cell viability were measured 9 to 12 h after treatment. (C) The levels of cell-cell fusion were quantified by counting syncytia. The minimum number of nuclei necessary to be considered a syncytium was 4 or more within a common cell membrane. Nuclei inside syncytia per random ×200 field were normalized to the no-treatment mock control, set at 100%. (D) Representative fields of syncytia, after treatment with 5 mM cholesterol/MβCD, circled in red. (E) The levels of CSE of NiV F after cholesterol enrichment were measured using polyclonal rabbit antibody 835 against NiV F. G was quantified using a monoclonal anti-HA PE antibody. After intercalation of membrane cholesterol, the levels of ephrinB2 binding to NiV G were measured with ephrinB2 fused to human Fc. (F) Representative Western blot analysis of NiV F expression and cleavage after cholesterol enrichment. Data shown are averages from three independent experiments ± SD. Statistical significance was determined with a one-sample t test. *, $P < 0.05$; **, $P < 0.01$; ***, $P < 0.001$; ****, $P < 0.0001$.

Effect of altering membrane cholesterol on NiV/VSV-pseudotyped virus entry.
As we found that the levels of NiV-induced cell-cell fusion were significantly altered by the concentration of membrane cholesterol, we then tested whether NiV entry into cells would also be affected. However, since NiV is a biosafety level 4 pathogen, we used our established biosafety level 2 NiV/vesicular stomatitis virus (VSV)-pseudotyped viral infection system to measure NiV entry. NiV/VSV-pseudotyped virions (NiV/VSV) carry a *Renilla* luciferase gene as a reporter for infectivity (41, 42, 45). We first asked whether cholesterol on the viral membranes would alter viral entry. The virions were treated with either MβCD (10 mM) or a cholesterol/MβCD mixture (5 mM) at 37°C for 30 min. While the depletion protocol reduced the levels of cholesterol in virions to ~30% ($P = 0.0094$), the enrichment protocol increased the levels of cholesterol in virions to ~140% compared to mock-treated NiV/VSV (set to 100%) (Fig. 3A). Notably, cholesterol depletion did not alter the amounts of F and G incorporated onto NiV/VSV. However, cholesterol enrichment reduced the amounts of F and G on NiV/VSV (Fig. 3B and C). The NiV/VSV particles were then serially diluted in infection buffer (PBS plus 1% bovine serum albumin [BSA]) and allowed to infect HEK293T cells for 2 h. Importantly, for all our viral entry assays, we used equal inputs of genome copies per infection. Genome copies were determined using quantitative reverse transcription-PCR, as we previously reported (41, 45). The levels of viral entry were quantified at 18 h postinfection, when luciferase expression was measured as relative light units (RLU), revealing that reducing the cholesterol concentration in the membrane significantly decreased viral infectivity (Fig. 3D) ($P < 0.01$). However, when considering the lower levels of incorporation of F and G on the virions (Fig. 3B and C), increasing the cholesterol concentration in the virions slightly increased viral infectivity (Fig. 3D). Altogether, our results indicated that the cholesterol-depleted viral particles yielded reduced levels, while the cholesterol-enriched virions yielded higher levels, of viral entry into cells.
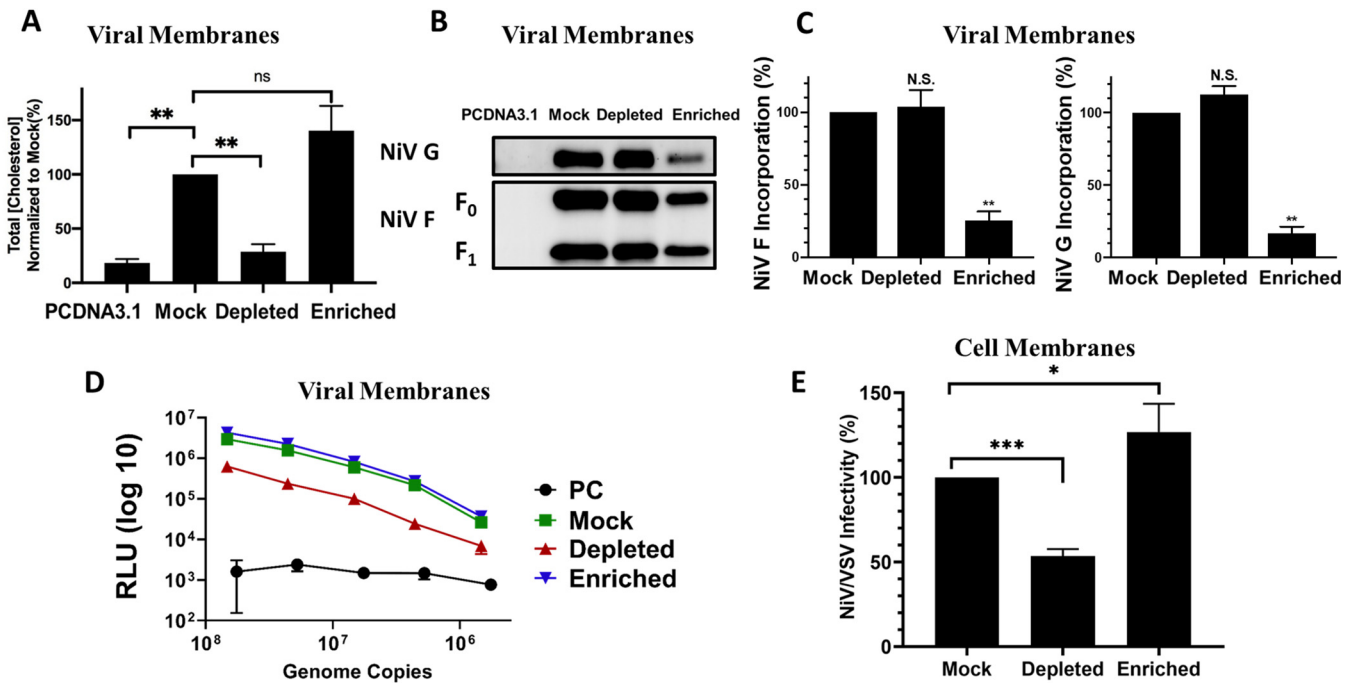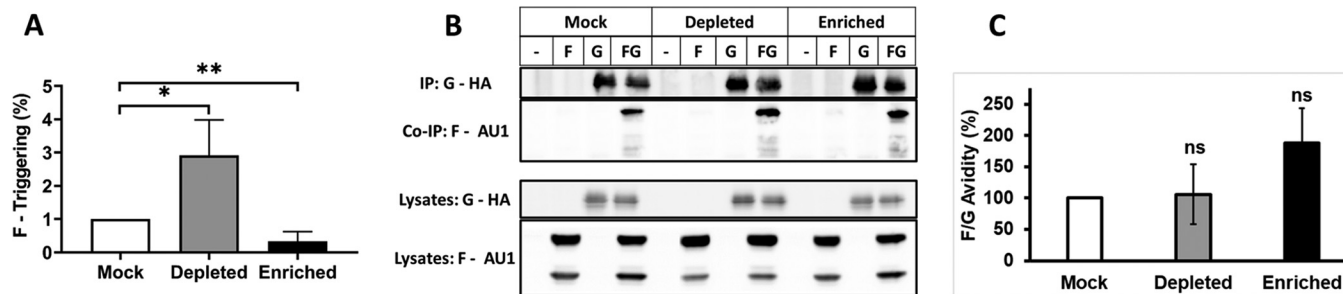
FIG 3 Modifying the concentration of membrane cholesterol alters viral particle infectivity. (A) The cholesterol concentration in NiV/VSV-pseudotyped virions, after treatment, was measured with an Amplex red cholesterol kit. Measurements were normalized to the mock-treated virus (set to 100%). (B) Western blot of NiV/VSV-pseudotyped virus from mock, cholesterol-depleted, and enriched NiV/VSV probed for NiV F/G glycoproteins. (C) Densitometry of NiV/VSV glycoproteins normalized to mock-treated NiV/VSV. PC, bald NiV/VSV produced with the pcDNA3.1(+) empty vector. Data shown are averages from three replicates ± SD. (D) Entry into HEK293T cells of NiV/VSV virions whose levels of cholesterol had been modified was measured with a *Renilla* luciferase kit (Promega). The RLU were quantified at 18 to 24 h postinfection. Data shown are from one representative of three independent experiments ± standard errors of the means (SEM). (E) Entry of NiV/VSV-pseudotyped virus into HEK293T target cells whose cholesterol levels had been modified. The data shown are averages from 4 independent experiments ± SD. Statistical significance was determined with a one-sample t test. *, $P < 0.05$; **, $P < 0.01$; ***, $P < 0.001$.

We then asked whether the concentration of membrane cholesterol in the target cells also affected NiV/VSV entry. We used our cholesterol depletion and enrichment protocols on the target HEK293T cells and then infected the cells for 2 h with NiV/VSV at a dilution of 1:4,000 (1.5×10^8 genome copies/ml), which yielded optimal luciferase activity without reducing cell viability. Measured over several orders of magnitude, we observed that depleting viral membrane cholesterol concentrations reduced viral infectivity levels (~40%) ($P = 0.0002$) compared to the mock control cells, while cholesterol-enriched target membranes significantly increased (~130%) ($P = 0.0497$) NiV/VSV infectivity (Fig. 3E), at equal genome copy levels. Altogether, our results suggest that membrane cholesterol in both the virus and host membrane influences NiV glycoprotein-mediated membrane fusion.

Effect of membrane cholesterol on the early NiV F-triggering step. Since we observed that the levels of both NiV-induced cell-cell and virus-cell membrane fusion were significantly altered by the concentration of membrane cholesterol, we then examined what step(s) during the NiV membrane fusion process was affected. We first tested whether the relatively early F-triggering step in the paramyxovirus membrane fusion process was altered. For this purpose, we used an F-triggering assay that we previously described (30, 41). Briefly, once G binds ephrinB2, G undergoes conformational changes that trigger F to transition from its prefusion state to its prehairpin intermediate (PHI) conformation, allowing F to insert its fusion peptide into the host membrane (31). The PHI can be captured with a Cy5-labeled peptide that mimics heptad repeat region 2 of NiV F (HR2-Cy5). To synchronize the membrane fusion process as much as possible, HEK293T cells transfected to express NiV F and G were collected at 12 to 14 h posttransfection, resuspended in PBS plus 1% BSA, and incubated for 90 min at 4°C with the NiV F HR2-Cy5 peptide. Incubation at 4°C allowed for G to bind to ephrinB2 but not for the temperature-dependent triggering of F to the PHI
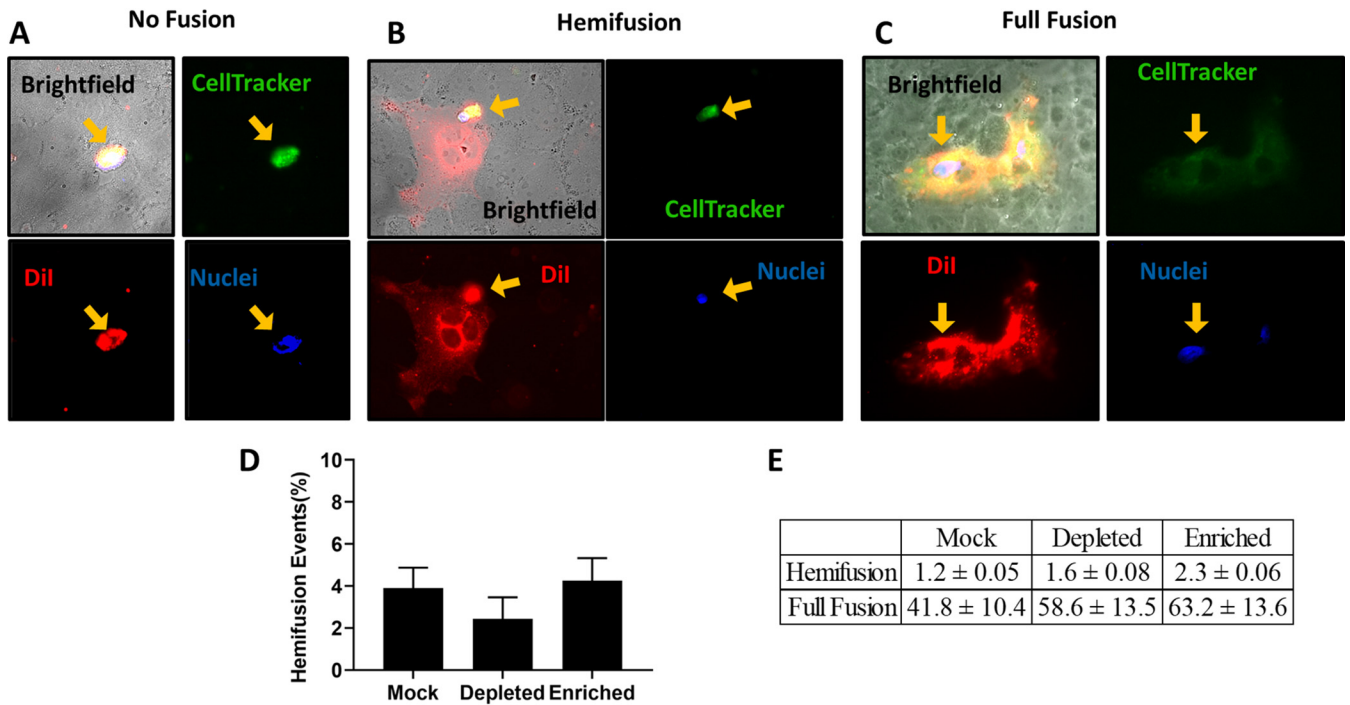
FIG 4 The concentration of membrane cholesterol affects the levels of NiV F triggering. The degree of NiV F triggering in cells with altered levels of membrane cholesterol was determined by the use of a NiV F HR2-Cy5 peptide. The peptide binds to the exposed HR1 during the PHI conformation after the transition from 4°C to 37°C. Averages from three independent experiments $\pm$ SD are shown. Statistical significance was determined with a one-sample t test. *, $P < 0.05$; **, $P < 0.01$. (B) Representative examples of a pulldown of NiV G (HA tagged) and coimmunoprecipitation (Co-IP) of F (Au1 tagged) in transfected HEK293T cells. (C) Avidity was quantified by Western blot densitometry. The levels were calculated as (IP F)/(CL F $\times$ IP G) (40, 46). CL, cell lysates. The averages from four replicates with standard errors are shown.

conformation and/or the F transition from PHI to 6HB to occur. The cells were then brought to 37°C for 30 min to allow F-triggering to occur, followed by cold PBS washing and fixation. The levels of HR2-Cy5 bound to the exposed NiV F HR2 in the PHI conformation were measured via flow cytometry. Since we observed a reduction in syncytium formation in cholesterol-depleted cells, we expected a decrease in the levels of F triggering. Interestingly, we observed an inverse correlation between the levels of syncytium formation and the levels of F triggering. The cholesterol-depleted cells had higher levels of F triggering ($P = 0.0170$), and the enriched cells had diminished levels of F triggering ($P = 0.0041$), compared to the mock control (Fig. 4). This suggests that a membrane with reduced levels of cholesterol allowed more NiV F triggering, and vice versa. Again, these results were counterintuitive compared to the cell-cell fusion levels obtained as a result of cholesterol depletion or enrichment (Fig. 1 and 2). Thus, we posited that an additional post-F-triggering step in the membrane fusion cascade must be affected by membrane cholesterol levels.

F4,AQ:C

Additionally, we performed a coimmunoprecipitation assay to determine if the concentration of membrane cholesterol altered the binding avidity of F and G. We pulled down NiV G with HA beads and coimmunoprecipitated Au1-tagged NiV F (Fig. 4B) (40, 46). We observed that the binding avidities between NiV F and G in cellular membranes with altered levels of cholesterol were not significantly different compared to those in mock-treated cells (Fig. 4C). Altogether, these results suggest that membrane cholesterol influences a late step in NiV membrane fusion.

Effect of membrane cholesterol on the late steps of the NiV membrane fusion cascade. During the membrane fusion cascade, after F triggering, a hemifusion step (fusion of the outer membrane leaflets of the two lipid bilayers) ensues before full-fusion pore formation and expansion occur (see Fig. 7). To determine if membrane cholesterol influences the levels of hemifusion, we performed a heterologous-cell fusion assay. This assay allowed us to discern the levels of outer leaflet merging between the effector and target membranes. PK13 cells, receptor negative for ephrinB2, were transfected to express F and G 24 h before treatment. Next, receptor-positive Vero cells, stained with CellTracker green, 1,1′-dioctadecyl-3,3,3′,3′-tetramethylindocarbocyanine perchlorate (DiI), and Hoechst stain to visualize their cytoplasm, plasma membrane, and nuclei, respectively, were overlaid onto the treated PK13 cells. The PK13 (effector) and Vero (target) cells were coincubated for 4 h at 37°C before being fixed with 2% paraformaldehyde (PFA). The proportions of hemifusion and full fusion were then quantified for all treatments. Examples of full-fusion and hemifusion events are shown (Fig. 5A to C). A nonfusion event (Fig. 5A) occurs when the stained Vero cell is situated on a monolayer of PK13 cells without the spread of the membrane dye DiI or the cytoplasmic marker CellTracker green. A hemifusion event (Fig. 5B) is characterized by the spreading of only DiI but not CellTracker green, which reveals that only the outer leaflets, but not the inner leaflets, of the cells have merged. A full-

A No Fusion

B Hemifusion

C Full Fusion

D

E

|	Mock	Depleted	Enriched
Hemifusion	1.2 ± 0.05	1.6 ± 0.08	2.3 ± 0.06
Full Fusion	41.8 ± 10.4	58.6 ± 13.5	63.2 ± 13.6

FIG 5 Heterologous cell-cell fusion upon cholesterol alteration. (A to C) PK13 cells were transfected with either pcDNA3.1(+) or NiV F/G expression plasmids. Vero cells were dyed with CellTracker green (top right), DiI (bottom right), and Hoechst stain (bottom left) (merged filters, along with bright-field images, are in the top left panel) to visualize their cytoplasm, plasma membrane, and nuclei, respectively, before being overlaid onto a monolayer of PK13 cells for 4 h before fixation with 0.5% paraformaldehyde. Examples of no fusion (A), hemifusion (B), and full fusion (C) are shown. (D) Hemifusion events (percent) from a 6-well plate were completely surveyed at a magnification of ×40 to determine relative levels of hemifusion and full-fusion events for each treatment. Data shown represent averaged ratios of hemifusion/full cell-cell fusion with standard errors. (E) Average hemifusion and full-fusion counts per well with standard errors ($n = 5$).

fusion event (Fig. 5C) is typified by the spread of both DiI and CellTracker green, which indicates that both leaflets of the target and effector membranes, as well as the cytoplasm, have merged. We observed that in effector cells with altered levels of membrane cholesterol, the amount of hemifusion was equal to that in the mock-treated cells (Fig. 5D). However, since the levels of F triggering were higher in the cholesterol-depleted cells, the progression to hemifusion must have been reduced if the overall levels of hemifusion were equal to those in the mock-treated cells. Conversely, since the levels of F triggering were lower in the cholesterol-enriched cells, the progression to hemifusion must have been greater if the overall levels of hemifusion were equal to those in mock-treated cells. Overall, these and the prior data imply that membrane cholesterol likely affects a critical posthemifusion step.

Membrane cholesterol affects NiV fusion pore formation. We then sought to determine whether later steps in the fusion cascade were altered, specifically fusion pore formation and fusion pore expansion. Thus, we performed a dual-split protein (DSP) assay in which the effector HEK293T cells were transfected with F, G, and half of the DSP construct composed of luciferase and green fluorescent protein (GFP) reporter chimeric proteins (47, 48). A construct containing the other halves of the DSP chimeric protein was transfected into the target HEK293T cells along with an empty vector, pcDNA3.1(+). Only when the two halves of the complex coalesce, upon fusion pore formation, could fluorescence or luminescence be detected. Importantly, this DSP assay is positive when a relatively small fusion pore forms, just large enough for the protein halves to mix (41). Using this DSP assay, we observed that decreasing membrane cholesterol levels resulted in reduced levels of NiV-induced fusion pore formation (10 mM) ($P = 0.0002$) (Fig. 6A). Conversely, when the concentration of membrane cholesterol was increased, we observed a significant increase in fusion pore formation (5 mM) ($P = 0.0120$) (Fig. 6B). These results most directly correlate with the phenotypes
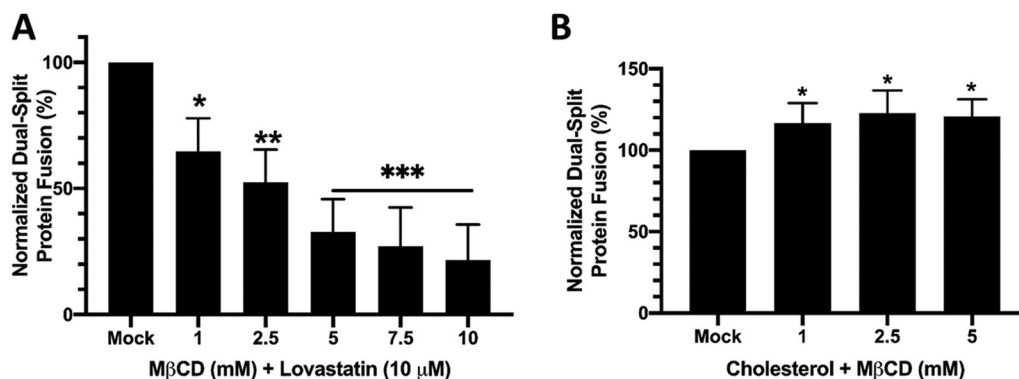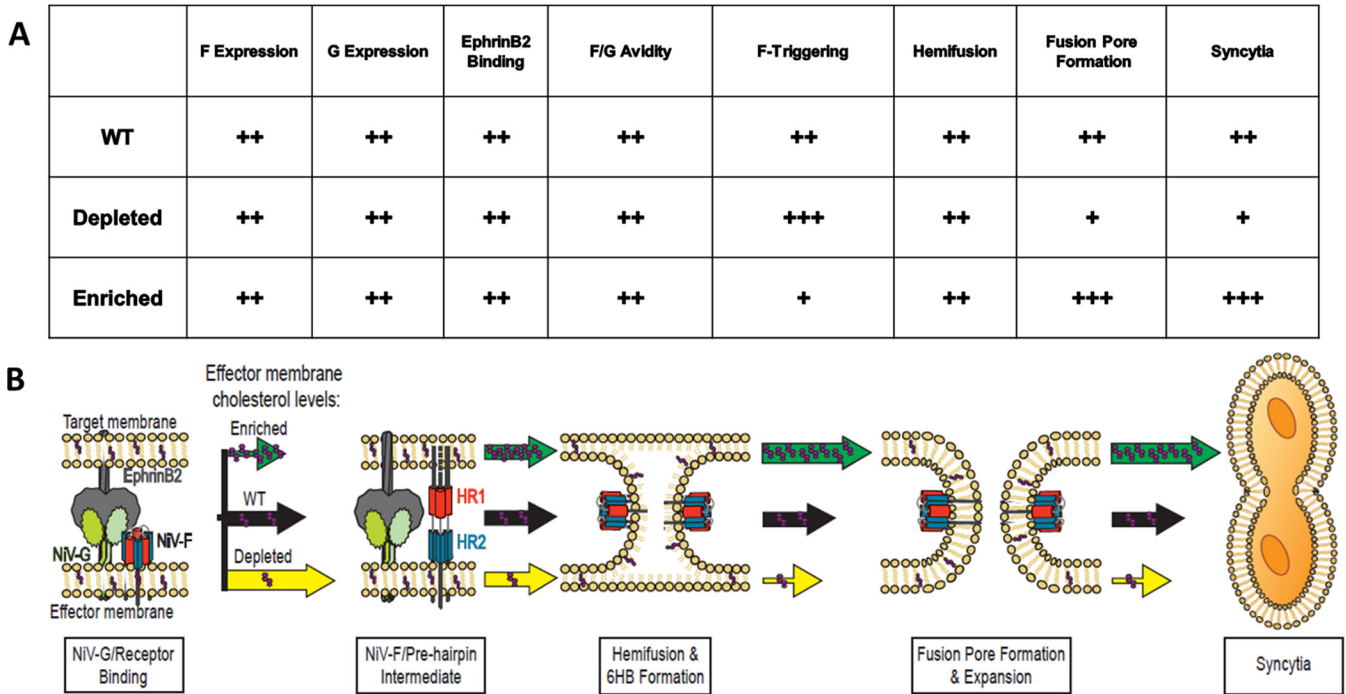
FIG 6 Modifying the concentration of membrane cholesterol alters fusion pore formation. The effector cells expressing NiV F/G and DSP1 were overlaid, after treatment, onto the target cells expressing DSP2. The degree of fusion pore formation, reported with the EnduRen live-cell substrate (Promega), was quantified at 8 to 12 h postoverlay in cholesterol-depleted (A) or cholesterol-enriched (B) cells. Data shown are averages from 3 independent experiments $\pm$ SD. Statistical significance was determined with a one-sample t test. *, $P < 0.05$; **, $P < 0.01$; ***, $P < 0.001$.

observed in our syncytium and viral entry experiments, suggesting that the fusion pore formation step is crucial for the results in these two important fusion assays.

DISCUSSION

The role of membrane cholesterol in viral fusion has remained unclear for the paramyxoviruses. Here, we report for the first time a mechanistic approach toward understanding the function of cholesterol in *Henipavirus* membrane fusion. Essentially, we observed that cholesterol depletion caused a significant increase in F triggering but a reduction in fusion pore formation and, ultimately, the formation of fewer syncytia (Fig. 1C and D, Fig. 4, and Fig. 6A). Conversely, with increased levels of membrane cholesterol, the levels of F triggering decreased, but the levels of fusion pore formation and the overall levels of syncytium formation increased (Fig. 2C and D, Fig. 4, and Fig. 6B). Altogether, our results suggest that the NiV fusion cascade is strongly influenced by the levels of membrane cholesterol and that fusion pore formation is key to the final fusion phenotype of the fusion cascade (Fig. 7A and B).

Several virology studies have utilized MβCD to transport membrane cholesterol solely to and from the plasma membrane. How these experiments were performed varied significantly. Differences in MβCD concentration, temperature, and duration of treatment are usually determined by the differences in cell lines (9, 11, 35). Therefore, we optimized our protocols to ensure that there was no negative effect on cell viability when our transfected HEK293T cells were treated with MβCD. Several studies have demonstrated that sequestration of cholesterol can have various effects on paramyxoviruses, such as the inhibition of cell-cell fusion, reduction of viral protein expression, and decreased infectivity of virus particles (14, 15, 17, 20, 37). Additionally, our new findings indicate that membrane cholesterol performs an essential mechanistic role in NiV fusion. Importantly, we observed that the expression of NiV F and G was not altered by a change in the level of membrane cholesterol (Fig. 1E and Fig. 2E). In contrast, expression levels of live human parainfluenza 1 and Sendai viruses were significantly reduced with cholesterol-reducing agents (37). Notably, our protocol did not affect the process of NiV F cleavage (Fig. 1F and Fig. 2F). Usually, the removal of membrane cholesterol hinders clathrin-mediated endocytosis, a process that generates the active, cleaved NiV fusion protein (49, 50). However, since we did not observe a decrease in NiV F cleavage, we speculate that the incubation period after MβCD treatment allowed for the reestablishment of endocytosis and for NiV F to be cleaved. Interestingly, a change in the level of membrane cholesterol did not alter the ability of NiV G to bind ephrinB2, even though some enveloped viruses that utilize host cell receptors for entry tend to display reduced levels of binding to cholesterol-depleted

A

	F Expression	G Expression	EphrinB2 Binding	F/G Avidity	F-Triggering	Hemifusion	Fusion Pore Formation	Syncytia
WT	++	++	++	++	++	++	++	++
Depleted	++	++	++	++	+++	++	+	+
Enriched	++	++	++	++	+	++	+++	+++

B

FIG 7 Summary table and model of the roles of membrane cholesterol in NiV membrane fusion. (A) The CSE of NiV F and G, the ability of NiV G to bind ephrinB2, and F/G binding avidity were not affected when membrane cholesterol was altered. However, the levels of F triggering were altered. An increase in membrane cholesterol reduced F triggering, while a reduction increased F triggering. However, the levels of hemifusion did not change with a change in the membrane cholesterol concentration. Nevertheless, a late step in NiV membrane fusion, fusion pore formation, was significantly altered. WT, wild type. (B) Model for the role of membrane cholesterol in NiV membrane fusion. NiV membrane fusion begins with the binding of G to ephrinB2, and this interaction induces conformation changes within G, which ultimately activates a conformational cascade in F. During F's transition from the PF to the PHI conformations, cholesterol-depleted cells (yellow arrow) had an increase in F triggering, while cholesterol-enriched cells (green arrow) had a reduction in F triggering, compared to mock-treated cells. Next, F merges the outer leaflets of the effector and target membranes. In cells with modified levels of cholesterol, the levels of quantified hemifusion events were not altered compared to mock-treated cells. NiV membrane fusion proceeds to fusion pore formation and expansion, which ultimately leads to viral entry or syncytium formation. Cholesterol-depleted cells yielded reduced levels, while cholesterol-enriched cells yielded high levels, of fusion pore formation compared to the mock cells. Overall, the cholesterol-depleted cells had reduced levels of syncytium formation, and the cholesterol-enriched cells had higher levels of cell-cell fusion. The sizes of the arrows indicate the relative levels of the phenotypes that they mark. Purple dots within the arrows represent the relative levels of cholesterol in those scenarios.

membranes, as was the case for HIV-1, NDV, and CDV (15, 17, 51), and the docking of RSV to target cells was dependent on cholesterol-rich domains (12).

We observed that decreasing levels of membrane cholesterol resulted in diminished levels of cell-cell fusion, while an increase in membrane cholesterol increased syncytium formation (Fig. 1C and Fig. 2C). A decrease in syncytium formation, due to cholesterol sequestration, was also observed among other enveloped viruses such as herpes simplex virus 1 (HSV-1), CDV, HIV-1, and influenza virus (9, 11, 17, 52) but interestingly not in cells infected by the paramyxovirus NDV (16). Similarly, an increase in cell-cell fusion, with the addition of exogenous cholesterol, was observed in HIV-1 and murine coronavirus infections (52, 53).

A reduction in the cholesterol concentration in the NiV/VSV particles (∼6-fold) (Fig. 3D) versus in the target cells (∼2-fold) (Fig. 3E) resulted in a reduction in viral entry. We speculate that this difference in the magnitude of the effect of cholesterol on viral infectivity when the levels of cholesterol are modified in the virus versus the target cell is due to differences in membrane lipid and protein compositions as well as membrane curvature. Conversely, NiV/VSV particles or target cells enriched in cholesterol displayed an increase in entry compared to mock-treated NiV/VSV and cells (Fig. 3). Indeed, the sensitivity of enveloped virus entry to the levels of membrane cholesterol is nearly ubiquitous (9, 11, 12, 15, 17, 54–56). However, the difference in infectivity, induced by an alteration of the cellular cholesterol concentration, may partly be due to the level of endocytosis, which has been shown to affect the internalization of RSV, NDV, and varicella-zoster virus (55, 57–59). Based on our results, a critical step in the

fusion cascade was impeded when membrane cholesterol was sequestered and enhanced with the addition of exogenous cholesterol. To determine the step(s) in the NiV fusion cascade influenced by the membrane cholesterol concentration, we performed several biochemical assays.

We observed that the triggering of NiV F was inversely proportional to the concentration of membrane cholesterol. This suggests that reducing the concentration of membrane cholesterol allows the NiV fusion machinery to be more readily activated and vice versa. Another possible explanation is that in a cholesterol-reduced membrane, triggered NiV F may be locked in the PHI conformation and unable to progress to the 6HB conformation to merge the membranes. The opposite may occur in cholesterol-enriched cells, where NiV F may undergo the transition from PF to PHI to 6HB at an accelerated rate, hence the higher levels of cell-cell fusion compared to mock-treated cells. This would be detected as a low-F-triggering phenotype in our F-triggering assay, as the F protein would live in the PHI for a shorter time. Nevertheless, our data suggest that the fusion cascade proceeds more readily with elevated levels of membrane cholesterol and less readily when membrane cholesterol is reduced. Interestingly, our findings differ from those obtained for the alphaviruses Semliki Forest virus and Sindbis virus, for which fusion protein triggering was promoted by cholesterol (60). We speculate that this may be due to differences in the conformational stabilities between the prefusion conformations of alphaviruses and paramyxoviruses. Additionally, we observed that the binding avidities between NiV F and G were not significantly altered in cells with altered levels of membrane cholesterol compared to mock-treated cells (Fig. 4B and C).

Furthermore, we tested whether the levels of hemifusion were influenced by membrane cholesterol. Using a heterologous-cell fusion assay, we observed equivalent levels of hemifusion. This indicates that in depleted cells, with greater levels of F-triggering, the transition to hemifusion from the PHI does not occur as readily, and vice versa. Nonetheless, the reductions or increases in syncytium formation (Fig. 1C and D and Fig 2C and D) were not due to inhibition or augmentation of the hemifusion step (Fig. 5D). In contrast to our findings, the levels of hemifusion and hemifusion stalk expansion were favored in high-cholesterol membranes during influenza virus fusion (61, 62).

We also investigated whether fusion pore formation was affected by cholesterol levels. For this purpose, we utilized a DSP system (41, 48), which has also been used to study fusion pore formation in HIV-1-induced cell-cell fusion (63). Using this assay, we observed that cholesterol depletion reduced the levels of NiV-induced fusion pore formation, while increased levels of membrane cholesterol generated higher levels of fusion pore formation (Fig. 6A and B). We speculate that this is due to the levels of flexibility of the membranes needed during fusion pore formation. Namely, decreased levels of membrane cholesterol may decrease the ability for the effector membrane to flex to form a fusion pore and vice versa.

In conclusion, we have revealed that NiV cell-cell and viral-cell membrane fusion was affected by the concentration of membrane cholesterol. Moreover, we demonstrated that the F-triggering and fusion pore formation steps during the NiV membrane fusion cascade are affected in opposite directions by the sequestration or intercalation of cholesterol, with fusion pore formation being a relatively more dominant phenotype for the overall cell-cell fusion phenotypic outcome. These roles reveal how components of the lipid bilayer affect the mechanism of NiV membrane fusion. However, it is not yet known whether this interaction of membrane cholesterol and viral kinetics is consistent in other paramyxoviruses or at least other henipaviruses. This study lays the foundation for potential studies of the roles of various membrane components and their effects on paramyxoviral and henipaviral infectivity.

MATERIALS AND METHODS

Cell culture. HEK293T, Vero, and PK13 (ATCC) cells were cultured in Dulbecco modified Eagle medium (Life Technologies) supplemented with 10% fetal bovine serum (FBS) and 1% penicillin-streptomycin (PenStrep) (Life Technologies). Cells were seeded on poly-L-lysine-coated plates before transfection.

Plasmids. Codon-optimized sequences for NiV F and G were inserted into pcDNA3.1 expression vectors and tagged with C-terminal Au1 and HA tags, respectively (GenBank accession numbers AY816748 and AY816745).

Modifying the membrane cholesterol concentration. For cholesterol depletion, HEK293T cells were incubated at room temperature for 1 h with the indicated concentrations of MβCD in serum-free medium. The cells were then washed with PBS. The cells were then incubated for an additional 9 to 12 h in serum-free medium with a 10 μM concentration of lovastatin or DMSO (vehicle control) (Sigma). For cholesterol enrichment, HEK293T cells were incubated at room temperature for 1 h with a solution of cholesterol/MβCD (1:20) (Sigma) in serum-free medium. Positive-control cells were treated with H_2O_2 at 0.3%. The cells were then washed multiple times with PBS and then incubated for an additional 9 to 12 h in serum-free medium. The total cholesterol concentration in cells was measured using the Amplex red cholesterol assay kit (Molecular Probes), according to the manufacturer's instructions. Cell viability was measured using cell-counting kit 8 (CCK-8), according to the manufacturer's instructions.

Syncytium quantification. HEK293T cells were seeded onto a 6-well plate and transfected when the monolayer was 80 to 90% confluent with 2 μg of F and G plasmids (3:1 ratio). Cells were treated with either MβCD or a cholesterol/MβCD ratio as described above 6 to 8 h after transfection when small syncytia became visible. Treatment was performed at room temperature for 1 h. The cells were then incubated with lovastatin or the DMSO control for an additional 12 h. Cells were then fixed with 2% PFA, and syncytium formation was quantified in at least 5 random fields per well, at a $\times$200 magnification (at least 15 fields per experimental condition). Syncytium formation was quantified by counting nuclei inside syncytia per field, whereby four or more nuclei within a cell were considered a syncytium (41, 64).

Quantification of NiV F and G cell surface expression and ephrinB2/G binding by flow cytometry. HEK293T cells, transfected and treated as described above, were collected at 15 to 18 h posttransfection. Cells were collected in PBS with 10 mM EDTA by cell scraping. Cells were then pelleted at 250 $\times$ *g* for 5 min at 4°C, resuspended in fluorescence-activated cell sorter (FACS) buffer (PBS plus 1% BSA), and aliquoted into a 96-well plate. Cells were then incubated with a polyclonal rabbit antibody (835) against NiV F (1:1,000), anti-HA phycoerythrin (PE) antibody to detect HA-tagged NiV G (1:500), and a soluble recombinant mouse ephrinB2/human Fc chimera (1:1,000) (R&D Systems, MN) for receptor binding detection, for 45 min at 4°C. Cells were then washed with PBS and incubated with anti-human Alexa Fluor 647 for ephrinB2 and anti-rabbit Alexa Fluor 647 (1:2,000) for F detection for 1 h at 4°C. Cells expressing NiV F, G, and ephrinB2 were labeled and analyzed in separate wells. Cells were then washed twice with PBS, fixed with 0.5% PFA in PBS, and analyzed on a Guava easyCyte 8HT benchtop flow cytometer (40, 41).

Pseudotyped virus production and quantification. Pseudotyped virions containing NiV F and NiV G were manufactured as previously described (45). Briefly, 15-cm plates of HEK293T cells were transfected at 37°C with NiV F and NiV G plasmids at a 3:1 ratio. Next, at 8 h posttransfection, cells were infected with recombinant VSV-ΔG-rLuc. Two hours later, the infection medium was removed, and the cells were either mock treated in serum-free medium or treated with MβCD. After treatment, the cells were incubated for an additional 36 h in serum-free medium with either the DMSO control or 10 μM lovastatin. The medium was cleared of debris by centrifugation at 250 $\times$ *g* for 10 min, concentrated on a 20% sucrose cushion in NaCl-Tris-EDTA (NTE) buffer for 90 min at 110,000 $\times$ *g* at 4°C, resuspended in NTE buffer with 5% sucrose, and stored at $-$80°C. Quantitative PCR (qPCR) was performed using a TaqMan probe for the VSV genome to quantify viral copy numbers as well as nanoparticle tracking analysis to confirm particle counts (42).

***Renilla* luciferase infectivity assays.** Wild-type NiV/VSV-pseudotyped virus was treated as stated above at 37°C for 30 min. The treated virus was then serially diluted in 1% BSA in PBS. The diluted virus was incubated with HEK293T cells in a 96-well plate for 2 h, followed by the addition of complete medium. The concentration of membrane cholesterol in HEK293T cells was altered as described above. The cells were then infected with wild-type NiV/VSV-pseudotyped virus for 2 h, followed by the addition of complete medium. At 18 to 24 h postinfection, cells were lysed using the *Renilla* luciferase assay (Promega). One hundred microliters of lysis buffer was added to each well, and the mixture was incubated for 10 min at $-$80°C. The cells were then placed in a rotating mixer for 20 min to thaw. Thirty microliters of the lysates was transferred to a transparent black-bottom 96-well plate (Costar). Fifty microliters of the substrate in assay buffer was added to each well, and luciferase activity was immediately measured using a Tecan Spark instrument (39, 42).

Heterologous cell-cell fusion assay. PK13 cells that are receptor negative for ephrinB2 were transfected with 2 μg of DNA (4:1 ratio of NiV F/G expression plasmids). PK13 target cells were cholesterol depleted or enriched in the manner described above. Vero cells were dyed with CellTracker green, DiI, and Hoechst stain to visualize their cytoplasm, plasma membrane, and nuclei, respectively, before overlaying. Vero cells were added to PK13 cells, spinoculated at 250 $\times$ *g* for 5 min, and incubated at 4°C for 45 min before being incubated for 4 h at 37°C. Cells were then fixed for 30 min in 0.5% paraformaldehyde in PBS.

F-triggering assay. HEK293T cells were transfected in 6-well plates (F/G ratio of 1,500 ng/500 ng) for 12 h. Cells were then washed with chilled PBS and resuspended in PBS plus 1% BSA. The HR2-Cy5 peptide was added to the cells to a final 2 μM concentration. Next, the cells were incubated at 4°C for 90 min with rotation to allow receptor binding, followed by a 30-min incubation at 37°C to allow F triggering. Next, cells were washed three times with FACS buffer (PBS plus 1% BSA). After the final wash, the cells were resuspended in FACS buffer and analyzed via flow cytometry to measure the levels of HR2-Cy5 binding (646 nm) to NiV F in the PHI conformation (30, 41).

Coimmunoprecipitation. Transfected cells were collected 18 h after cholesterol alteration. Cells were lifted in cold PBS with a cell scraper. The cell pellet was lysed with 200 μl of lysis buffer and incubated on a rotating mixer for 30 min at 4°C. Thirty microliters of HA decorated microbeads was added to 100 μl of the lysates, and the remaining lysates were analyzed via Western blotting. The cell lysate and microbead mixture was then loaded onto a microcolumn and washed with 2 ml of lysis buffer, followed by a single wash with low-salt wash buffer. Protein was eluted off the column with warm elution buffer and quantified via Western blotting (40, 46).

Dual-split protein fusion assay. HEK293T cells in a 12-well plate were transfected with 1,200 μg of DNA with F-G-DSP1 (3:1:2). Only the effector cells were treated as described above. The target HEK293T cells were seeded onto a Perkin-Elmer glass-bottom flat black plate. The target cells were transfected with 200 μg pcDNA3.1-DSP2 (2:1). The cells were treated at 12 h posttransfection, as described above. The cells were collected and overlaid onto the target cells in the presence of 10 μM EnduRen (Promega) in serum-free medium. The cells were allowed to fuse at 37°C, and luminescence was detected 8 to 12 h later. Relative light units (RLU) were normalized to the values for mock-treated cells (41).

ACKNOWLEDGMENTS

REFERENCES

1. Chazal N, Gerlier D. 2003. Virus entry, assembly, budding, and membrane rafts. Microbiol Mol Biol Rev 67:226–237. https://doi.org/10.1128/mmbr.67.2.226-237.2003.

2. Verma DK, Gupta D, Lal SK. 2018. Host lipid rafts play a major role in binding and endocytosis of influenza A virus. Viruses 10:650. https://doi.org/10.3390/v10110650.

3. Suomalainen M. 2002. Lipid rafts and assembly of enveloped viruses. Traffic 3:705–709. https://doi.org/10.1034/j.1600-0854.2002.31002.x.

4. Campbell SM, Crowe SM, Mak J. 2001. Lipid rafts and HIV-1: from viral entry to assembly of progeny virions. J Clin Virol 22:217–227. https://doi.org/10.1016/s1386-6532(01)00193-7.

5. Waheed AA, Freed EO. 2009. Lipids and membrane microdomains in HIV-1 replication. Virus Res 143:162–176. https://doi.org/10.1016/j.virusres.2009.04.007.

6. Nguyen DH, Hildreth JE. 2000. Evidence for budding of human immunodeficiency virus type 1 selectively from glycolipid-enriched membrane lipid rafts. J Virol 74:3264–3272. https://doi.org/10.1128/jvi.74.7.3264-3272.2000.

7. Guyader M, Kiyokawa E, Abrami L, Turelli P, Trono D. 2002. Role for human immunodeficiency virus type 1 membrane cholesterol in viral internalization. J Virol 76:10356–10364. https://doi.org/10.1128/jvi.76.20.10356-10364.2002.

8. Liao Z, Graham DR, Hildreth JE. 2003. Lipid rafts and HIV pathogenesis: virion-associated cholesterol is required for fusion and infection of susceptible cells. AIDS Res Hum Retroviruses 19:675–687. https://doi.org/10.1089/088922203322280900.

9. Wudiri GA, Schneider SM, Nicola AV. 2017. Herpes simplex virus 1 envelope cholesterol facilitates membrane fusion. Front Microbiol 8:2383. https://doi.org/10.3389/fmicb.2017.02383.

10. Wudiri GA, Nicola AV. 2017. Cellular cholesterol facilitates the postentry replication cycle of herpes simplex virus 1. J Virol 91:e00445-17. https://doi.org/10.1128/JVI.00445-17.

11. Sun X, Whittaker GR. 2003. Role for influenza virus envelope cholesterol in virus entry and infection. J Virol 77:12543–12551. https://doi.org/10.1128/jvi.77.23.12543-12551.2003.

12. San-Juan-Vergara H, Sampayo-Escobar V, Reyes N, Cha B, Pacheco-Lugo L, Wong T, Peeples ME, Collins PL, Castaño ME, Mohapatra SS. 2012. Cholesterol-rich microdomains as docking platforms for respiratory syncytial virus in normal human bronchial epithelial cells. J Virol 86:1832–1843. https://doi.org/10.1128/JVI.06274-11.

13. Chang T-H, Segovia J, Sabbah A, Mgbemena V, Bose S. 2012. Cholesterol-rich lipid rafts are required for release of infectious human respiratory syncytial virus particles. Virology 422:205–213. https://doi.org/10.1016/j.virol.2011.10.029.

14. Laliberte JP, McGinnes LW, Peeples ME, Morrison TG. 2006. Integrity of membrane lipid rafts is necessary for the ordered assembly and release of infectious Newcastle disease virus particles. J Virol 80:10652–10662. https://doi.org/10.1128/JVI.01183-06.

15. Martin JJ, Holguera J, Sanchez-Felipe L, Villar E, Munoz-Barroso I. 2012. Cholesterol dependence of Newcastle disease virus entry. Biochim Biophys Acta 1818:753–761. https://doi.org/10.1016/j.bbamem.2011.12.004.

16. Dolganiuc V, McGinnes L, Luna EJ, Morrison TG. 2003. Role of the cytoplasmic domain of the Newcastle disease virus fusion protein in association with lipid rafts. J Virol 77:12968–12979. https://doi.org/10.1128/jvi.77.24.12968-12979.2003.

17. Imhoff H, von Messling V, Herrler G, Haas L. 2007. Canine distemper virus infection requires cholesterol in the viral envelope. J Virol 81:4158–4165. https://doi.org/10.1128/JVI.02647-06.

18. Li LY, Yu LY, Hou XL. 2017. Cholesterol-rich lipid rafts play a critical role in bovine parainfluenza virus type 3 (BPIV3) infection. Res Vet Sci 114:341–347. https://doi.org/10.1016/j.rvsc.2017.04.009.

19. Tang QP, Liu PF, Chen MZ, Qin YL. 2019. Virion-associated cholesterol regulates the infection of human parainfluenza virus type 3. Viruses 11:438. https://doi.org/10.3390/v11050438.

20. Fujita H, Tamai K, Kawachi M, Saga K, Shimbo T, Yamazaki T, Kaneda Y. 2011. Methyl-beta cyclodextrin alters the production and infectivity of Sendai virus. Arch Virol 156:995–1005. https://doi.org/10.1007/s00705-011-0938-7.

21. Drexler JF, Corman VM, Müller MA, Maganga GD, Vallo P, Binger T, Gloza-Rausch F, Cottontail VM, Rasche A, Yordanov S, Seebens A, Knörnschild M, Oppong S, Adu Sarkodie Y, Pongombo C, Lukashev AN, Schmidt-Chanasit J, Stöcker A, Carneiro AJB, Erbar S, Maisner A, Fronhoffs F, Buettner R, Kalko EKV, Kruppa T, Franke CR, Kallies R, Yandoko ERN, Herrler G, Reusken C, Hassanin A, Krüger DH, Matthee S, Ulrich RG, Leroy EM, Drosten C. 2012. Bats host major mammalian paramyxoviruses. Nat Commun 3:796. https://doi.org/10.1038/ncomms1796.

22. Spiropoulou CF. 2019. Nipah virus outbreaks: still small but extremely lethal. J Infect Dis 219:1855–1857. https://doi.org/10.1093/infdis/jiy611.

23. Sharma V, Kaushik S, Kumar R, Yadav JP, Kaushik S. 2019. Emerging trends of Nipah virus: a review. Rev Med Virol 29:e2010. https://doi.org/10.1002/rmv.2010.

24. Ang BSP, Lim TCC, Wang L. 2018. Nipah virus infection. J Clin Microbiol 56:e01875-17. https://doi.org/10.1128/JCM.01875-17.

25. Negrete OA, Levroney EL, Aguilar HC, Bertolotti-Ciarlet A, Nazarian R, Tajyar S, Lee B. 2005. EphrinB2 is the entry receptor for Nipah virus, an emergent deadly paramyxovirus. Nature 436:401–405. https://doi.org/10.1038/nature03838.

26. Aguilar HC, Ataman ZA, Aspericueta V, Fang AQ, Stroud M, Negrete OA, Kammerer RA, Lee B. 2009. A novel receptor-induced activation site in the Nipah virus attachment glycoprotein (G) involved in triggering the fusion glycoprotein (F). J Biol Chem 284:1628–1635. https://doi.org/10.1074/jbc .M807469200.

27. Liu Q, Stone JA, Bradel-Tretheway B, Dabundo J, Montano JAB, Santos-Montanez J, Biering SB, Nicola AV, Iorio RM, Lu XN, Aguilar HC. 2013. Unraveling a three-step spatiotemporal mechanism of triggering of receptor-induced Nipah virus fusion and cell entry. PLoS Pathog 9:e1003770. https://doi.org/10.1371/journal.ppat.1003770.

28. Liu Q, Bradel-Tretheway B, Monreal AI, Saludes JP, Lu XN, Nicola AV, Aguilar HC. 2015. Nipah virus attachment glycoprotein stalk C-terminal region links receptor binding to fusion triggering. J Virol 89:1838–1850. https://doi.org/10.1128/JVI.02277-14.

29. Stone JA, Vemulapati BM, Bradel-Tretheway B, Aguilar HC. 2016. Multiple strategies reveal a bidentate interaction between the Nipah virus attachment and fusion glycoproteins. J Virol 90:10762–10773. https://doi.org/ 10.1128/JVI.01469-16.

30. Aguilar HC, Aspericueta V, Robinson LR, Aanensen KE, Lee B. 2010. A quantitative and kinetic fusion protein-triggering assay can discern distinct steps in the Nipah virus membrane fusion cascade. J Virol 84:8033–8041. https://doi.org/10.1128/JVI.00469-10.

31. Aguilar HC, Henderson BA, Zamora JL, Johnston GP. 2016. Paramyxovirus glycoproteins and the membrane fusion process. Curr Clin Microbiol Rep 3:142–154. https://doi.org/10.1007/s40588-016-0040-8.

32. Wong KT, Shieh WJ, Kumar S, Norain K, Abdullah W, Guarner J, Goldsmith CS, Chua KB, Lam SK, Tan CT, Goh KJ, Chong HT, Jusoh R, Rollin PE, Ksiazek TG, Zaki SR, Nipah Virus Pathology Working Group. 2002. Nipah virus infection—pathology and pathogenesis of an emerging paramyxoviral zoonosis. Am J Pathol 161:2153–2167. https://doi.org/10.1016/S0002 -9440(10)64493-8.

33. Huang H, Li Y, Sadaoka T, Tang H, Yamamoto T, Yamanishi K, Mori Y. 2006. Human herpesvirus 6 envelope cholesterol is required for virus entry. J Gen Virol 87:277–285. https://doi.org/10.1099/vir.0.81551-0.

34. Desplanques AS, Nauwynck HJ, Vercauteren D, Geens T, Favoreel HW. 2008. Plasma membrane cholesterol is required for efficient pseudorabies virus entry. Virology 376:339–345. https://doi.org/10.1016/j.virol.2008.03 .039.

35. Zidovetzki R, Levitan I. 2007. Use of cyclodextrins to manipulate plasma membrane cholesterol content: evidence, misconceptions and control strategies. Biochim Biophys Acta 1768:1311–1324. https://doi.org/10 .1016/j.bbamem.2007.03.026.

36. Stancu C, Sima A. 2001. Statins: mechanism of action and effects. J Cell Mol Med 5:378–387. https://doi.org/10.1111/j.1582-4934.2001 .tb00172.x.

37. Bajimaya S, Hayashi T, Frankl T, Bryk P, Ward B, Takimoto T. 2017. Cholesterol reducing agents inhibit assembly of type I parainfluenza viruses. Virology 501:127–135. https://doi.org/10.1016/j.virol.2016.11.011.

38. Laliberte JP, McGinnes LW, Morrison TG. 2007. Incorporation of functional HN-F glycoprotein-containing complexes into Newcastle disease virus is dependent on cholesterol and membrane lipid raft integrity. J Virol 81:10636–10648. https://doi.org/10.1128/JVI.01119-07.

39. Stone JA, Nicola AV, Baum LG, Aguilar HC. 2016. Multiple novel functions of henipavirus O-glycans: the first O-glycan functions identified in the Paramyxovirus family. PLoS Pathog 12:e1005445. https://doi.org/10.1371/ journal.ppat.1005445.

40. Johnston GP, Contreras EM, Dabundo J, Henderson BA, Matz KM, Ortega V, Ramirez A, Park A, Aguilar HC. 2017. Cytoplasmic motifs in the Nipah virus fusion protein modulate virus particle assembly and egress. J Virol 91: e02150-16. https://doi.org/10.1128/JVI.02150-16.

41. Bradel-Tretheway BG, Zamora JLR, Stone JA, Liu Q, Li J, Aguilar HC. 2019. Nipah and Hendra virus glycoproteins induce comparable homologous but distinct heterologous fusion phenotypes. J Virol 93:e00577-19. https://doi.org/10.1128/JVI.00577-19.

42. Bradel-Tretheway BG, Liu Q, Stone JA, McInally S, Aguilar HC. 2015. Novel functions of Hendra virus G N-glycans and comparisons to Nipah virus. J Virol 89:7235–7247. https://doi.org/10.1128/JVI.00773-15.

43. Barman S, Nayak DP. 2007. Lipid raft disruption by cholesterol depletion enhances influenza A virus budding from MDCK cells. J Virol 81:12169–12178. https://doi.org/10.1128/JVI.00835-07.

44. Chen Y, Ott CJ, Townsend K, Subbaiah P, Aiyar A, Miller WM. 2009. Cholesterol supplementation during production increases the infectivity of retroviral and lentiviral vectors pseudotyped with the vesicular stomatitis virus glycoprotein (VSV-G). Biochem Eng J 44:199–207. https://doi.org/10 .1016/j.bej.2008.12.004.

45. Aguilar HC, Matreyek KA, Filone CM, Hashimi ST, Levroney EL, Negrete OA, Bertolotti-Ciarlet A, Choi DY, McHardy I, Fulcher JA, Su SV, Wolf MC, Kohatsu L, Baum LG, Lee B. 2006. N-glycans on Nipah virus fusion protein protect against neutralization but reduce membrane fusion and viral entry. J Virol 80:4878–4889. https://doi.org/10.1128/JVI.80.10.4878-4889 .2006.

46. Aguilar HC, Matreyek KA, Choi DY, Filone CM, Young S, Lee B. 2007. Polybasic KKR motif in the cytoplasmic tail of Nipah virus fusion protein modulates membrane fusion by inside-out signaling. J Virol 81:4520–4532. https://doi.org/10.1128/JVI.02205-06.

47. Nakane S, Matsuda Z. 2015. Dual split protein (DSP) assay to monitor cell-cell membrane fusion. Methods Mol Biol 1313:229–236. https://doi.org/ 10.1007/978-1-4939-2703-6_17.

48. Atanasiu D, Saw WT, Gallagher JR, Hannah BP, Matsuda Z, Whitbeck JC, Cohen GH, Eisenberg RJ. 2013. Dual split protein-based fusion assay reveals that mutations to herpes simplex virus (HSV) glycoprotein gB alter the kinetics of cell-cell fusion induced by HSV entry glycoproteins. J Virol 87:11332–11345. https://doi.org/10.1128/JVI.01700-13.

49. Diederich S, Sauerhering L, Weis M, Altmeppen H, Schaschke N, Reinheckel T, Erbar S, Maisner A. 2012. Activation of the Nipah virus fusion protein in MDCK cells is mediated by cathepsin B within the endosome-recycling compartment. J Virol 86:3736–3745. https://doi.org/10.1128/JVI .06628-11.

50. Rodal SK, Skretting G, Garred O, Vilhardt F, van Deurs B, Sandvig K. 1999. Extraction of cholesterol with methyl-beta-cyclodextrin perturbs formation of clathrin-coated endocytic vesicles. Mol Biol Cell 10:961–974. https://doi.org/10.1091/mbc.10.4.961.

51. Ono A, Waheed AA, Freed EO. 2007. Depletion of cellular cholesterol inhibits membrane binding and higher-order multimerization of human immunodeficiency virus type 1 Gag. Virology 360:27–35. https://doi.org/ 10.1016/j.virol.2006.10.011.

52. Liao Z, Cimakasky LM, Hampton R, Nguyen DH, Hildreth JE. 2001. Lipid rafts and HIV pathogenesis: host membrane cholesterol is required for infection by HIV type 1. AIDS Res Hum Retroviruses 17:1009–1019. https://doi .org/10.1089/088922201300343690.

53. Thorp EB, Gallagher TM. 2004. Requirements for CEACAMs and cholesterol during murine coronavirus cell entry. J Virol 78:2682–2692. https:// doi.org/10.1128/jvi.78.6.2682-2692.2004.

54. Graham DRM, Chertova E, Hilburn JM, Arthur LO, Hildreth JEK. 2003. Cholesterol depletion of human immunodeficiency virus type 1 and simian immunodeficiency virus with beta-cyclodextrin inactivates and permeabilizes the virions: evidence for virion-associated lipid rafts. J Virol 77:8237–8248. https://doi.org/10.1128/jvi.77.15.8237 -8248.2003.

55. Hambleton S, Steinberg SP, Gershon MD, Gershon AA. 2007. Cholesterol dependence of varicella-zoster virion entry into target cells. J Virol 81:7548–7558. https://doi.org/10.1128/JVI.00486-07.

56. Saeed MF, Kolokoltsov AA, Albrecht T, Davey RA. 2010. Cellular entry of Ebola virus involves uptake by a macropinocytosis-like mechanism and subsequent trafficking through early and late endosomes. PLoS Pathog 6: e1001110. https://doi.org/10.1371/journal.ppat.1001110.

57. Kolokoltsov AA, Deniger D, Fleming EH, Roberts NJ, Jr, Karpilow JM, Davey RA. 2007. Small interfering RNA profiling reveals key role of clathrin-mediated endocytosis and early endosome formation for infection by respiratory syncytial virus. J Virol 81:7786–7800. https://doi.org/10 .1128/JVI.02780-06.

58. Gutiérrez-Ortega A, Sánchez-Hernández C, Gómez-García B. 2008. Respiratory syncytial virus glycoproteins uptake occurs through clathrin-mediated endocytosis in a human epithelial cell line. Virol J 5:127. https://doi .org/10.1186/1743-422X-5-127.

59. Tan L, Zhang Y, Zhan Y, Yuan Y, Sun Y, Qiu X, Meng C, Song C, Liao Y, Ding C. 2016. Newcastle disease virus employs macropinocytosis and Rab5a-dependent intracellular trafficking to infect DF-1 cells. Oncotarget 7:86117–86133. https://doi.org/10.18632/oncotarget.13345.

60. Umashankar M, Sánchez-San Martín C, Liao M, Reilly B, Guo A, Taylor G, Kielian M. 2008. Differential cholesterol binding by class II fusion proteins determines membrane fusion properties. J Virol 82:9245–9253. https:// doi.org/10.1128/JVI.00975-08.

61. Biswas S, Yin S-R, Blank PS, Zimmerberg J. 2008. Cholesterol promotes hemifusion and pore widening in membrane fusion induced by influenza hemagglutinin. J Gen Physiol 131:503–513. https://doi.org/10.1085/jgp .200709932.

62. Chlanda P, Mekhedov E, Waters H, Schwartz CL, Fischer ER, Ryham RJ, Cohen FS, Blank PS, Zimmerberg J. 2016. The hemifusion structure induced by influenza virus haemagglutinin is determined by physical properties of the target membranes. Nat Microbiol 1:16050. https://doi.org/10.1038/nmicrobiol.2016.50.

63. Yamamoto M, Du Q, Song J, Wang H, Watanabe A, Tanaka Y, Kawaguchi Y, Inoue JI, Matsuda Z. 2019. Cell-cell and virus-cell fusion assay-based analyses of alanine insertion mutants in the distal alpha9 portion of the JRFL gp41 subunit from HIV-1. J Biol Chem 294:5677–5687. https://doi.org/10.1074/jbc.RA118.004579.

64. Johnston GP, Bradel-Tretheway B, Piehowski PD, Brewer HM, Lee BNR, Usher NT, Zamora JLR, Ortega V, Contreras EM, Teuton JR, Wendler JP, Matz KM, Adkins JN, Aguilar HC. 2019. Nipah virus-like particle egress is modulated by cytoskeletal and vesicular trafficking pathways: a validated particle proteomics analysis. mSystems 4:e00194-19. https://doi.org/10.1128/mSystems.00194-19.